Luminescence properties of dual valence Eu doped nano-crystalline BaF_2 embedded glass-ceramics and observation of $Eu^{2+} \rightarrow Eu^{3+}$ energy transfer

Kaushik Biswas, Atul D. Sontakke, R. Sen, K. Annapurna*
Glass Science and Technology Section, Central Glass and Ceramic Research Institute,
Council of Scientific and Industrial Research
196, Raja S.C. Mullick Road, Kolkata – 700 032, India.

Abstract

Europium doped glass ceramics containing BaF_2 nano-crystals have been prepared by using the controlled crystallization of melt-quenched glasses. X-ray diffraction and transmission electron microscopy have confirmed the presence of cubic BaF_2 nano-crystalline phase in glass matrix in the ceramized samples. Incorporation of rare earth ions into the formed crystalline phase having low phonon energy of 346 cm^{-1} has been demonstrated from the emission spectra of Eu^{3+} ions showing the transitions from upper excitation states ^5D_J (J = 1, 2, and 3) to ground states for the glass-ceramics samples. The presence of divalent europium ions in glass and glass-ceramics samples is confirmed from the dominant blue emission corresponding to its *5d-4f* transition under an excitation of 300 nm. Increase in the reduction of trivalent europium (Eu^{3+}) ions to divalent (Eu^{2+}) with the extent of ceramization is explained by charge compensation model based on substitution defect mechanisms. Further, the phenomenon of energy transfer from Eu^{2+} to Eu^{3+} ion by radiative trapping or re-absorption is evidenced which increases with the degree of ceramization. For the first time, the reduction of Eu^{3+} to Eu^{2+} under normal air atmospheric condition has been observed in a BaF_2 containing oxyfluoride glass-ceramics system.

Keywords: Glasses, Transparent oxyfluoride glass ceramics, Optical probe, Eu-Luminescence

*Corresponding author: Tel: +91-33-2473 3469; Fax: +91-33-2473 0957
Email: annapurnak@cgcri.res.in (K. Annapurna)

INTRODUCTION

Among various rare earth ions, europium doped materials are both scientifically and technically relevant with great importance due to their efficient and intense fluorescence [1-3]. Europium can exist in both divalent (Eu^{2+}) and trivalent (Eu^{3+}) forms depending upon the host material or environment during synthesis of the material. Eu^{3+} doped materials are widely used in the display devices as efficient red emitting phosphors, field emission devices, and solid state lasers [4-6]. Further, Eu^{3+} is widely used as a spectral probe to study the local crystal field due to its $^5D_0 \rightarrow {}^7F_2$ forced electric-dipole transition, which is hypersensitive to any changes in the chemical surroundings of the luminescent active ions [7]. On the other hand, in Eu^{2+} doped material, the emission due to $4f^7$-$4f^6 5d$ transition is partially-allowed and that occurs with a high transition probability. Depending on the covalency of host-matrix, size of cation and strength of crystal field, the emission of Eu^{2+} varies from ultraviolet to red region [8-9]. Eu^{2+}-doped phosphor materials are potential candidates for white-light-emitting diodes when it is pumped by ultraviolet sources [10]. However, Eu^{2+} is chemically metastable in an oxidizing atmosphere and is prone to oxidation via $Eu^{2+} \rightarrow Eu^{3+} + e^-$. To synthesize Eu^{2+}-doped materials starting with Eu_2O_3 as raw material, Eu^{3+} is reduced to Eu^{2+} in a reducing atmosphere such as H_2, H_2/N_2 or CO [11-12]. The reduction of Eu^{3+} to Eu^{2+} could also be realized by γ-ray irradiation in alkaline earth sulphates and femtosecond laser irradiation in fluorozirconate glass [13-15]. However, there are reports on the reduction process of Eu^{3+} to Eu^{2+} in non-reducing atmosphere. The reduction of Eu^{3+} ions under normal atmospheric condition has been observed in borate, phosphate, aluminate, borophosphate, sulfate, silicate and alumnioborosilicate based systems [16]. But there is no thorough study on the reduction of Eu^{3+} to Eu^{2+} in oxyfluoride glass systems under non-reducing condition.

Recently, Luo et al. studied the reduction process for Eu doped SiO_2-Al_2O_3- SrF_2- NaF glass system [17]. In their study, the presence of Eu^{2+} was not evidenced in melt-quenched oxyfluoride glass prepared under normal atmosphere. However, blue luminescence of Eu^{2+} ions has been reported in glass ceramics samples containing SrF_2 nano-crystals indicating a reduction process of Eu^{3+} to Eu^{2+} during ceramization. Later, the same group has reported the presence of Eu^{2+} in oxyfluoride glasses containing BaF_2 nano-crystals synthesized under reducing atmosphere [18]. In both the studies, the emission spectra of Eu^{2+} ions were recorded under the excitation wavelength of Eu^{3+} ions instead of using the excitation wavelength of Eu^{2+} ions without proper explanation for the selection of such excitation.

Oxyfluoride glass and glass-ceramics are promising host material for several active optical applications because these glasses combine low phonon energy due to fluorides environment, and high chemical durability with superior mechanical stability in an oxide environment [19-24]. Due to the low phonon energy sites of alkaline-earth fluoride nano-crystallites (300-400 cm^{-1}), they exhibit efficient fluorescent properties with an enhanced emission efficiency and longer lifetimes because of the reduced non-radiative relaxations and possess high solubility of both sensitizer and activator rare earth ions. Recently, the photoluminescence properties of Pr^{3+} doped SiO_2–BaF_2–K_2CO_3–La_2O_3-Sb_2O_3 based transparent oxyfluoride glass and glass-ceramics containing BaF_2 nano-crystals have been studied by our group [25]. In this glass system, SiO_2 takes the role of glass network former while BaF_2, K_2O, and La_2O_3 being network modifies and Sb_2O_3 acts as refining agent. In particular, La_2O_3 has been considered in the present system mainly to facilitate the substitution of dopant lanthanides. In the present work, europium was considered as a structural probe to investigate the local environment around rare-earth ions in the same oxyfluoride glass composition synthesized under normal atmospheric condition. In addition,

the effect of ceramization on the coexistence of Eu^{2+} and Eu^{3+} in glass-ceramics has been compared with glass samples through the analysis of their excitation and emission spectra.

EXPERIMENTAL

Oxyfluoride glasses in the composition of (mol %) 68 SiO_2–15 BaF_2–13 K_2CO_3–2.75 La_2O_3-1.0 Sb_2O_3-0.25 Eu_2O_3 were prepared by melt-quenching method using high purity raw chemicals such as SiO_2 (99.8%, Sipur A1 Bremtheler Quartzitwerk, Usingen, Germany), BaF_2 (99.99 %, Merck KgaA, Darmstadt, Germany), K_2CO_3 (99.9 %, Loba Chemie Pvt. Ltd., Mumbai, India), La_2O_3 (99.9 % Alfa Aesar, Ward Hill, MA), Sb_2O_3 (99.9 %, Merck KgaA, Darmstadt, Germany) and Eu_2O_3 (99.99%, Alfa Aesar**,** Karlsruhe, Germany). The chemical batches for about 30 g glass were prepared by thorough mixing and were melt in pure platinum crucible with lid in an open air atmosphere furnace at 1450^{o}C for 1 h. Homogenization of the molten glass was performed by stirring at regular intervals and then the melt was cast onto a preheated graphite mould, followed by annealing at 450^{o}C for 1 h with subsequent slow cooling to the room temperature to relinquish the internal stresses. Later, the glass samples were heat-treated at 600^{o}C (labeled as GC1) and 650^{o}C (labeled as GC2) temperatures for 24 h duration. Precursor glass samples are termed as sample G now onwards for convenience. These glass and glass-ceramics samples were cut to the desired sizes and processed for carrying out further characterization.

Refractive indices (*n*) of the samples were measured at five wavelengths of 473 nm, 532 nm, 633 nm, 1064 nm, and 1552 nm on a Prism Coupler (Metricon Model-2010, NJ, USA) fitted with five different lasers as illuminating sources. The densities (*d*) of the samples were measured by Archimedes' principle using water as buoyancy liquid on Mettler Tollado

balance fitted with density measurement kit. The X-ray diffraction (XRD) patterns were recorded using an X'pert Pro MPD diffractometer (PANalytical, Almelo, The Netherlands) using X'Celerator operating at 40kV and 30 mA using Ni-filtered CuKα radiation with wavelength of 1.5418367 Å. The data was acquired in step-scan mode with step size 0.05^0 (2θ) and step time 50 sec from 10^0 to 80^0. The microstructure of the glass ceramic samples was investigated by transmission electron microscope (FEI Model Tecnai G2 30ST, Hillsboro, OR, USA), samples for TEM measurement were prepared by dispersing finely powdered glasses in ethanol, followed by an ultrasonic agitation, and then its deposition onto the carbon-enhanced copper grid.

The optical absorption spectra were recorded using Perkin Elmer UV–Vis spectrophotometer (Model Lambda 20, Perkin Elmer, Waltham, MA, USA) in the wavelength range 300–1100 nm. The steady state emission and excitation spectra were carried out on a fluorescence spectrophotometer (Quantum Master-enhanced NIR from Photon Technologies International, USA) fitted with double monochromators on both excitation and emission channels using continuous Xenon arc lamp as excitation source of 75 W and liquid nitrogen cooled NIR-PMT R1.7 Hamamatsu as fluorescence detector. All the measurements were carried out by placing the samples at 60^0 to the incident beam and the resulted signals were collected from the same surface at right angle to the incident beam. The acquisition of the spectral data was performed using PTI FeliX32 software.

RESULTS AND DISCUSSION

Physical and optical properties

The precursor glass (G) and glass ceramic samples (GC1 and GC2) are shown in Fig. 1. It is evident from this figure that, a visual inspection of precursor glass and GC1 sample

are observed to be quite transparent, while GC2 sample is slightly translucent. The measured refractive indices at five wavelengths for all the samples are summarized in Table I along with measured density, average molecular weight and other related properties. These values have been used to compute refractive indices ($n_{F'}$, n_e, $n_{C'}$) at standard wavelengths of $\lambda_{F'}$ = 480 nm, λ_e = 546.1 nm and $\lambda_{C'}$ = 643.8 nm by Sellmeier fitting and the dispersion curves thus obtained are represented in Figure 2. As, BaF_2 has a lower refractive index compared to the precursor glass, the refractive indices of glass-ceramic samples tend to decrease with the increase in the degree of ceramization [25]. Table I also shows that there is a decrease in the density of samples upon ceramization. The decrease in density can be attributed to an increase in the number of non-bridging oxygen in the residual glass matrix upon ceramization of BaF_2 nano-crystals which causes an expansion of the volume of overall glass network. Furthermore, it can be noticed from Table I that the rare earth ion concentration, inter-ionic distance and field strength do not change appreciably for glass and glass ceramic samples.

Structural Characterization

The X-ray diffraction pattern of the as-quenched glass (sample G) in Fig. 3 has revealed broad halos confirming its amorphous nature. In contrary, GC1 and GC2 samples exhibited distinct diffraction peaks which are in agreement with face centered cubic (fcc) barium fluoride (BaF_2) crystalline phase having space group *Fm -3m* (ICSD code: 041649) and are indexed appropriately in Fig. 3. The TEM bright field images of glass-ceramic samples are shown in Figs. 4 (a) and (b). From these figures, homogeneously distributed spherical crystallites (in dark appearance) in the glass matrices are clearly evident. The size of these crystallites ranges from 6-10 nm for GC1 sample ceramized at 600^0C (Fig. 4 (a)), whereas it is observed to be 10-20 nm for GC2 sample ceramized at 650^0C (Fig. 4 (b)). This indicates that the BaF_2 nano-crystallites, which nucleate below 600^0C, grow with the increase

in ceramization temperature causing translucency in GC2 sample. The insets of both the figures display the selected area electron diffraction (SAED) pattern with bright concentric rings occurring from the diffraction planes of identified polycrystalline phase.

Optical absorption spectra

The UV-VIS optical absorption spectra of the glass and glass-ceramic samples are presented in Fig. 5. In both the samples, ten absorption peaks have been revealed in the wavelength range of 350-625 nm which are attributed to the $4f \rightarrow 4f$ transitions from ground state multiplets $^7F_{0,1}$ to different excited states of Eu^{3+} ions in $4f^6$ configuration. The inset of Fig. 5 displays a magnified view of the absorption spectra showing very sharp, intense and well-defined peaks. The peaks at 577 nm, 526 nm, 462 nm, 415 nm, 393 nm, 381 nm and 362 nm are the transitions from ground state $^7F_0$ to several excited states of $^5D_0$, $^5D_1$, $^5D_2$, $^5D_3$, $^5L_6$, $^5G_{2,4}$ and $^5D_4$, respectively of Eu^{3+} ions. Three small absorption bands with peaks at 588 nm, 533 nm and 400 nm occur due to the transitions from thermally excited ground state multiplet $^7F_1$ to $^5D_0$, $^5D_1$, and $^5L_6$ excited states respectively and those are marked with asterisks in Fig. 5. Normally, $^7F_1$ level remains sufficiently populated even at room temperature due to its close proximity with ground state, $^7F_0$ with an energy gap of around 350 cm^{-1}. It is also noticed from this figure that, there is a red shift of UV band edge for the ceramized samples. This can be attributed to the spread of localized density of states just below the conduction band of the arising with the presence of dopant ions. That is, the superimposition of absorption transition at around 350-500 nm from $4f^7 \rightarrow 4f^6 5d$ of Eu^{2+} ions with fundamental host absorption which is corroborated from the recorded excitation spectra discussed in subsequent section. In comparison to this transition, $f \rightarrow f$ absorption peaks of Eu^{3+} are relatively weak in intensity due to their parity forbidden nature. The peak corresponding to

$^7F_0 \rightarrow {}^5L_6$ transition is the most intense among all other recorded absorption bands which can be used for the excitation of Eu^{3+} ions.

Emission and Excitation Spectra

Fig. 6 depicts the photoluminescence spectra of all samples obtained upon excitation at 394 nm ($^7F_0 \rightarrow {}^5L_6$). The spectra exhibit characteristic emission peaks between 570 nm and 750 nm wavelengths due to transitions within the $4f^6$ configuration of Eu^{3+}. The spectra of all samples are dominated by an intense red emission at 610 nm due to the $^5D_0 \rightarrow {}^7F_2$ forced electric-dipole transition. The other emission peaks have been assigned to $^5D_0 \rightarrow {}^7F_0$ (579 nm), $^5D_0 \rightarrow {}^7F_1$ (591 nm), $^5D_0 \rightarrow {}^7F_3$ (652 nm), and $^5D_0 \rightarrow {}^7F_4$ (703 nm) transitions of the Eu^{3+} ions. The inset of the figure clearly demonstrates the bright red luminescence from GC2 sample under 394 nm wavelength of excitation. Unlike the precursor glass, the ceramized samples have revealed emission peaks in the wavelength range of 410 - 560 nm those have resulted due to the transitions from upper excitation states ^5D_J (J = 1, 2, and 3) in addition to the transitions from $^5D_0$ to ground level multiplets. This can be elucidated as a result of the incorporation of Eu^{3+} ions in embedded BaF_2 nano-crystals of lower phonon energy (~346 cm^{-1}) in glass matrix compared to precursor oxyfluoride glass (~1000 cm^{-1}). In GC1 and GC2 samples, because of the low phonon energy in the fluoride nano-crystal environment, the cascading of upper ^5D_J excited levels to $^5D_0$ level through multi-phonon relaxation becomes reduced causing enhanced radiative emission probability directly from ^5D_J levels to ground state multiplets in comparison to glass.

The excitation spectra recorded by monitoring 610 nm wavelength corresponding to the red emission of Eu^{3+} ($^5D_0 \rightarrow {}^7F_2$) for all the samples are shown in Fig. 7. The spectra exhibit a broad band from 240 to 350 nm having main peak maximum at 300 nm along side with the overlap of two sharp peaks (at 306 and 322 nm) on it. In addition to these, a number of sharp peaks have also been revealed in 350-600 nm wavelength range. The sharp peaks

correspond to the transitions from ground state to excited states within the $4f^6$ configuration of Eu^{3+} ions which are appropriately assigned based on their peak energies. In the case of broad band, its origin can be speculated either due to the charge transfer band of Eu^{3+} ions or due to the transition from *4f* ground state ($^8S_{7/2}$) to *5d* level of Eu^{2+} ions. In order to understand the exact nature of the broad excitation band, emission spectra were recorded by exciting the samples at 300 nm wavelength and are shown in Fig. 8. The spectra exhibit sharp peaks in the wavelength range 570 - 720 nm along with intense broad emission band peaking at 388 nm. The sharp peaks in the longer wavelengths have been assigned to $^5D_0 \rightarrow {}^7F_{0\text{-}4}$ of Eu^{3+} ions. The presence of the dominant broad band at lower wavelength region rules out the possibility of occurrence of charge transfer band (CTB) of Eu^{3+} ions in Fig. 7. This is because of the fact that, the broad emission band is not expected if the excitation band would have been originated from charge transfer band of Eu^{3+}. Thus, the broad emission band may be attributed to the characteristic $4f^6 5d \rightarrow 4f^7$ transition of Eu^{2+} ions. From the spectra, it is evident that, even the precursor glasses have demonstrated the presence of divalent europium ions (Eu^{2+}) and moreover, there is no much change in Eu^{2+} luminescence in the sample ceramized at 600^0C for 24 hrs (GC1 sample) in comparison to precursor glass with a mere 1.08 (8%) increase of intensity. But the increase in Eu^{2+} emission intensity for GC2 sample is clearly evident which is enhanced by 1.4 times (40%) compared to precursor glass sample. Also, it is observed that the relative intensity ratio of Eu^{2+} emission to that of Eu^{3+} ions increases with the extent of crystallization, which indicates the reduction of Eu^{3+} to Eu^{2+} during ceramization process. Its value in GC2 sample is 2.25 whereas for precursor glass sample, it is 2.01. This observation establishes that, though the formation of Eu^{2+} during the glass preparation itself takes place, further reduction of Eu^{3+} to Eu^{2+} progresses during ceramization event. Thus, in glass-ceramic samples, it is to consider that, the contribution of

dopant ions (Eu^{3+}, Eu^{2+}) embedded in both BaF_2 nanocrystals and residual glass-matrix influences overall emission intensity.

Moreover, in the emission spectra, noticeable emission from Eu^{3+} ions is detected in addition to Eu^{2+} blue emission under 300 nm wavelength excitation of Eu^{2+} ions (Fig. 8). This can be due to direct excitation of Eu^{3+} because some of the higher excited states of Eu^{3+} are overlapped with the broadband (e.g. $^5F_2$, $^5H_6$) as shown in Fig. 7. Therefore, these levels may directly get populated when the sample is excited with 300 nm. Upon direct excitation, the intensity of Eu^{3+} emission is expected to be characteristically very weak from those higher excited states (e.g. $^5F_2$, $^5H_6$). Hence, the noticed intense Eu^{3+} emission rules out the possibility of only direct excitation. The other possibility of this observation could be energy transfer from Eu^{2+} to Eu^{3+}. Upon ceramization, due to reduction of Eu^{3+} to Eu^{2+}, the intensity of Eu^{3+} is expected to decrease. In contrary, it is observed that the intensities of both Eu^{2+} and Eu^{3+} emission increase simultaneously upon ceramization. This is interpreted as follows: a part of energy might be transferred to Eu^{3+} from Eu^{2+}. This speculation is corroborated from the presence of a distinct kink in the Eu^{2+} emission at 394 nm (marked in Fig. 8), which is the absorption wavelength of Eu^{3+}. Though the presence of the kink is distinct in GC2 sample, a critical examination over the spectra shows its presence even in precursor glass and GC1 sample. This is an experimental evidence of radiative resonant energy transfer from Eu^{2+} to Eu^{3+}. Thus, this energy transfer from $Eu^{2+} \rightarrow Eu^{3+}$ could be realized in the present study due to the close matching of Eu^{2+} emission peak wavelength (388 nm) with that of Eu^{3+} absorption (393 nm).

As mentioned earlier, the relative intensity ratio of Eu^{2+} emission to that of Eu^{3+} ions increases with the extent of crystallization, which indicates the reduction of Eu^{3+} to Eu^{2+} during ceramization process. This can be explained by the charge compensation model based

on substitution defect mechanisms [16, 26]. This model describes that when trivalent Eu^{3+} ions replace Ba^{2+} ions, to keep the charge neutrality, two Eu^{3+} ions substitute for three Ba^{2+} ions to form a cation vacancy, a $Eu_{Ba}^{\bullet}$ defect with two negative charges ($V_{Ba}^{''}$). While, the $Eu_{Ba}^{\bullet}$ defect becomes an acceptor of electron, $V_{Ba}^{''}$ defects act as donor of electron. Subsequently, the negative charges in the vacancy defects tend to transfer to the Eu^{3+} site causing the reduction of Eu^{3+} ions to Eu^{2+} ions. Thus, this reduction phenomenon brings about the incorporation of Eu^{2+} into BaF_2 nanocrystalline phase. The charge compensation model can be explained by the following defect equations:

$$3Ba_{Ba} + 2Eu^{3+} = 3Ba^{2+} + 2Eu_{Ba}^{\cdot} + V_{Ba}^{''}$$
$$V_{Ba}^{''} = V_{Ba}^{X} + 2e^{'}$$
$$2Eu_{Ba}^{\cdot} + 2e^{'} = 2Eu_{Ba}^{X}$$

Though there is significant reduction of Eu^{3+} ions to Eu^{2+} ions in the base glass composition during high temperature synthesis under oxidizing atmosphere, the reduction process is extended with precipitation of BaF_2 upon ceramization due to thermal stimulation causing a enhanced Eu^{2+}: Eu^{3+} ratio compared to glass samples. For the first time to our knowledge, the reduction of Eu^{3+} to Eu^{2+} in normal atmospheric condition is evidenced in this oxyfluoride glass and glass-ceramics system. In oxyfluoride glass, the silicate network is interrupted at places by replacement of bridging oxygen with non-bridging fluorine. Additionally, there could be a small fraction of fluorine atoms linked to the SiO_4 tetrahedral without any rupture of the Si-O network with fivefold coordinated silicon [27]. The presence of non-bridging oxygen and non-bridging fluorine favors the higher positively charged cations (e.g, Eu^{3+}) to neutralize the negative charges provided by non-bridging atoms [28]. However, in the present glass, Eu^{2+} ions in a three-dimensional four fold and five fold coordinated rigid network are

less likely to be re-oxidized by oxygen and fluorine compared to glasses having plane rings or chain structure [16]. During ceramization, the incorporation of Eu^{2+} ions into the cubic BaF_2 crystals reduces the possibility of presence of non-bridging oxygen or fluorine in the vicinity of Eu^{2+} ions. Thus, the Eu^{2+} ions become more stable with the increase in ceramization. With the increase of Eu^{2+} formation during ceramization, the transfer of energy from Eu^{2+} to Eu^{3+} takes place predominantly. Consequently, instead of expected increase in the intensity Eu^{2+} blue emission, the increase Eu^{3+} red emission is also observed. As a result, the glass ceramic samples have exhibited bright pink color (a mixture of blue and red) luminescence under Eu^{2+} excitation as shown in the inset of Fig. 8.

Energy transfer mechanism

To understand the energy transfer mechanism from Eu^{2+} to Eu^{3+} in more clarity, a configuration coordinate diagram for the Eu^{2+} and Eu^{3+} ions has been presented for GC2 sample in Fig. 9 along with their emission and excitation spectra. The configuration coordinate diagram clearly demonstrates the occurrence of energy transfer phenomenon from Eu^{2+} to Eu^{3+} ions in which the radiated energy from excited levels of Eu^{2+} ions to their ground state is readily transferred to the ground state Eu^{3+} ions and those are excited to $^5L_6$ state. This is due to the close matching of emission energy of Eu^{2+} to that of excitation energy of the $^5L_6$ state of Eu^{3+} ion from which cascading of energy occurs down to the $^5D_0$ level followed by radiative transitions to $^7F_0$, $^7F_1$, $^7F_2$, $^7F_3$ and $^7F_4$ levels. This is evidenced by the presence of a kink at 394 nm in the Eu^{2+} emission spectra monitored at λ_{ex} = 300 nm. This is the possible reason for the observation of considerable Eu^{3+} emission under Eu^{2+} excitation at 300 nm.

CONCLUSIONS

In summary, it could be concluded that the photoluminescence properties of europium doped BaF_2 containing oxyfluoride based glass-ceramics have successfully been analyzed and compared with a precursor glass. The precursor glass has been prepared from the standard melt quenching method. The obtained glasses have been subjected to subsequent heat-treatment in achieving the formation of glass-ceramics for carrying out their structural and luminescence characterizations. X-ray diffraction (XRD) and transmission electron microscopy (TEM) analysis have confirmed the formation of cubic BaF_2 nano-crystallites embedded in glass matrix. The glass and glass-ceramic samples have exhibited bright red fluorescence upon Eu^{3+} excitation (395 nm). Further, the presence of higher energy emission peaks from $^5D_{3,\ 2,\ 1}$ levels of Eu^{3+} ions in the Eu doped BaF_2 glass-ceramics confirmed the incorporation of Eu^{3+} ions into the BaF_2 nano-crystals of low phonon energy. The measured excitation and emission spectra have confirmed the coexistence of both Eu^{3+} and Eu^{2+} ions in all the samples. Moreover, reduction of Eu^{3+} to Eu^{2+} ions progressed upon ceramization which has been explained on the basis of charge neutrality. Additionally, evidence of energy transfer from Eu^{2+} to Eu^{3+} is observed in the glass-ceramic samples due to radiative trapping or re-absorption resulting in mixed pink color fluorescence under Eu^{2+} excitation (300 nm).

Acknowledgement

Authors would like to thank Prof. I. Manna, Director, CGCRI for his kind encouragement and permission to publish this work that was carried out in an In-house project No. OLP-0288. One of us (Mr.A.D.S.) is thankful to the BRNS-DAE for the award of Junior Research Fellowship to him.

References

[1] J. S. Bae, J. H. Juong, S.-S. Yi, and J. -C. Park, (2003), Improved photoluminescence of pulsed-laser-ablated $Y_2O_3:Eu^{3+}$ thin-film phosphors by Gd substitution, *Appl. Phys. Lett.* **82**(21), 3629–3631.

[2] X.-X. Wang, J. Wang, J.-X. Shi, Q. Su, and M.-L. Gong, (2007), Intense red-emitting phosphors for LED solid-state lighting, *Mater. Res. Bull.* **42**(9), 1669–1673.

[3] X. Zhao, X.Wang, B. Chen, Q. Meng, W. Di, G. Ren, and Y. Yang, (2007), Novel Eu^{3+}-doped red-emitting phosphor $Gd_2Mo_3O_9$ for white-light-emitting-diodes (WLEDs) applications, *J. Alloys Compd.* **433**(1-2), 352–355.

[4] H.M. Yang, J.X. Shi, and M.L. Gong, (2005), A novel red-emitting phosphor $Ca_2SnO_4:Eu^{3+}$, *J. Solid State Chem.* **178**(3), 917–920.

[5] R.P. Rao and D.J. Devine, (2000), RE-activated lanthanide phosphate phosphors for PDP applications, *J. Lumin.* **87–89**, 1260–1263.

[6] A. Poloman, (1997), Erbium implanted thin film photonic materials, *J. Appl. Phys.* **82**(1), 1–39.

[7] E.W.J.L. Oomen and A.M.A. van Dongen, (1989), Europium (III) in oxide glasses: Dependence of the emission spectrum on glass composition, *J. Non-Crystalline Solids* **111**(2-3), 205–213.

[8] P. Dorenbos, (2003), Energy of the first $4f^7 - 4f^6 5d$ transition of Eu^{2+} in inorganic compounds, *J. Lumin.* **104**(4), 239–260.

[9] S.H.M. Poort, H.M. Reijhoudt, H.O.T. van der Kuip, W. Janssen and G. Blasse, (1996), Luminescence of Eu^{2+} in silicate host lattices with alkaline earth ions in a row, *J. Alloys Compd.* **241**(1-2), 75–81.

[10] J.S. Kim, P.E. Jeon, Y.H. Park, J.C. Choi, and H.L. Park, (2004), White-light generation through ultraviolet-emitting diode and white-emitting phosphors, *Appl. Phys. Lett.* **85**(17), 3696–3698.

[11] L.-T. Chen, C.-S. Hwang, I.-G. Chen, and S.-J. Chang, (2006), Chromaticity of inhomogeneous broadening effect on $Ca_xSr_{1-x}Al_2O_4$: Eu^{2+}, *J. Alloy. Compd.* **426**(1-2), 395–399.

[12] G. A. Hirata, F. E. Ramos, and J. McKittrick, (2005), Development of luminescent materials with strong UV-blue absorption, *Opt. Mater.* **27**(7), 1301–1304.

[13] X. Gong, P. Wu, W. Chan, and W. Chen, (2000), The dependence of conductivity of cellulose, silk and wool on their water content, *J. Phys. Chem. Solids* **16**(1-2), 115–121.

[14] V.N. Bapat, (1977), Thermoluminescence process in $CaSO_4$:Eu, *J. Phys. C: Solid State Phys.* **10**(16), L465–L467.

[15] J. Qiu, K. Kojima, T. Miura, T. Mitsuyu, and K. Hirao, (1999), Infrared femtosecond laser pulse induced permanent reduction of Eu^{3+} to Eu^{2+} in a fluorozirconate glass, *Opt. Lett.* **24**(11), 786–788.

[16] Z. Lian, J. Wang, Y.H. Lv, S.B. Wang, and Q. Su, (2007), The reduction of Eu^{3+} to Eu^{2+} in air and luminescence properties of Eu^{2+} activated $ZnO–B_2O_3–P_2O_5$ glasses *J. Alloys Compd.* **430** (1-2) 257–261.

[17] Q. Luo , X. Qiao, X. Fan, S. Liu, H. Yang, and X. Zhang, (2008), Reduction and luminescence of Europium ions in glass ceramics containing SrF_2 nanocrystals, *J. Non-Crystalline Solids* **354**(40-41), 4691–4694.

[18] Q. Luo, X. Fan, X. Qiao, H. Yang, and M. Wang, (2009), Eu^{2+} doped glass-ceramics containing BaF_2 nanocrystals as a potential blue phosphor for UV-LED, *J. Am. Ceram. Soc.* **92**(4), 942–944.

[19] M. Mortier, P. Goldner, C. Chateau, and M. Genotelle, (2001), Erbium doped glass-ceramics: concentration effect on crystal structure and energy transfer between active ions, *J. Alloys Compd.* **323-324**, 245–249.

[20] Y. Wang, and J. Ohwaki, (1993), New transparent vitroceramics codoped with Er^{3+} and Yb^{3+} for efficient frequency upconversion, *Appl. Phys. Lett.* **63**(24), 3268–3270.

[21] M. J. Dejneka, (1998), Transparent oxyfluoride glass-ceramics, *MRS Bull.* **23**, 57–62.

[22] M. J. Dejneka, (1998), The luminescence and structure of novel oxyfluoride glass-ceramics, *J. Non-Cryst. Solids* **239**(1-3), 149–155.

[23] T. Honma, M. Kusatsugu, and T. Komatsu, (2009), Synthesis of LaF_3 nanocrystals by laser-induced Nd^{3+} atom heat processing in oxyfluoride glasses, *Mater. Chem. Phys.* **113**(1), 124–129.

[24] D. Chen, Y. Wang, Y. Yu, E. Ma, F. Bao, Z. Hu, and Y. Cheng, (2006), Influence of Er^{3+} content on structure and upconversion emission of oxyfluoride glass ceramics containing CaF_2 nanocrystals, *Mater. Chem. Phys.* **95**(2-3), 264–269.

[25] K. Biswas, A. D. Sontakke, J. Ghosh, and K. Annapurna, (2010), Enhanced blue emission from transparent oxyfluoride glass-ceramics containing Pr^{3+}:BaF_2 nanocrystals, *J. Am. Ceram. Soc.* **93**(4), 1010–1017.

[26] M.Y. Peng, Z.W. Pei, G.Y. Hong, and Q. Su, (2003), Study on the reduction of $Eu^{3+} \rightarrow Eu^{2+}$ in $Sr_4Al_{14}O_{25}$:Eu prepared in air atmosphere, *Chem. Phys. Lett.* **371**(1-2), 1–6.

[27] R. E. Youngman, and S. Sen, (2004), The nature of fluorine in amorphous silica, *J. Non-Cryst. Solids* **337**(2) 182–186.

[28] C. Wang, M. Peng, N. Jiang, X. Jiang, and C. Zhao, J. Qiu, (2007), Tuning the Eu luminecsnence in glass materials synthesized in air by adjusting glass composition, *Mater. Lett.* **61**(17), 3608–3611.

Figure captions:

Figure 1: Photograph of the (a) as-prepared glass and glass ceramic samples ceramized at (b) 600^{o}C and (c) 650^{o}C for 24 h.

Figure 2: Dispersion curves of glass and glass ceramic samples that are heat treated at different temperatures.

Figure 3: X-ray diffraction patterns of glass and glass-ceramic samples.

Figure 4: TEM image of (a) GC1 and (b) GC2 samples. Inset shows the SAED pattern of BaF_2 crystals embedded in glass matrix.

Figure 5: Absorption spectra of precursor (a) glass (G) and (b) glass-ceramic (GC1) samples.

Figure.6: Emissions spectra of BaF_2: Eu containing glass and glass-ceramic samples on excitation with 394 nm.

Figure 7: Excitation spectra of BaF_2: Eu containing glass and glass-ceramic samples on monitoring the 610 nm emission.

Figure 8: Emissions spectra of BaF_2: Eu containing glass and glass-ceramic samples on excitation with 300 nm.

Figure 9: Configuration coordination diagram for Eu^{2+} and Eu^{3+} energy levels.

Table I. Different physical, optical properties of precursor glass (G) and glass ceramic samples (GC1 and GC2).

Properties		**Samples**		
		G	GC1	GC2
Average molecular weight		97.9	97.9	97.9
Density, g cm^{-3}		3.24	3.20	3.20
Refractive Indices	**473 nm**	1.5575	1.5557	1.5531
	532 nm	1.5531	1.5510	1.5486
	632.8 nm	1.5481	1.5460	1.5439
	1064 nm	1.5388	1.5356	1.5342
	1552 nm	1.5336	1.5302	1.5294
Mean dispersion $(n_{F'}-n_{C'})$		0.0093	0.0092	0.0091
Abbe number $(n_E-1)/(n_{F'}-n_{C'})$		59.4	59.8	60.2
Reflection loss, R%		4.682	4.655	4.624
Molar refractivity, R_M, cm^3		9.796	9.889	9.854
Molecular electronic polarizability, α_e, cm^3 ($\times 10^{-24}$)		3.885	3.922	3.908
Rare earth concentration, N, (ions/cm^3) ($\times 10^{21}$)		9.967	9.844	9.844
Ionic radius, r_p, Å		1.905	1.913	1.913
Inter-ionic distance, r_i, Å		5.501	5.524	5.524
Field Strength, F, cm^2($\times 10^{15}$)		8.270	8.202	8.202

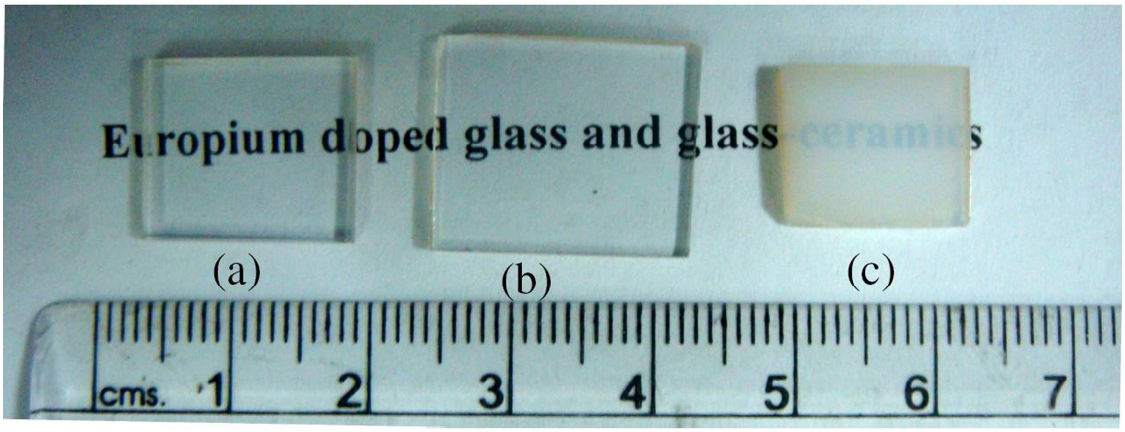

Fig. 1

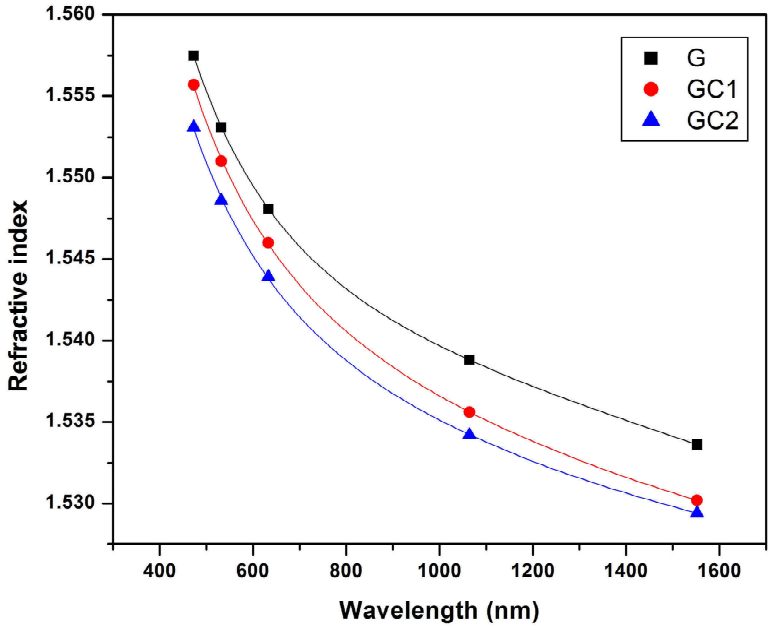
1.560
1.555
1.550
1.545
1.540
1.535
1.530
Refractive index
400
600
800
1000
1200
1400
1600
Wavelength (nm)
G
GC1
GC2

Fig. 2

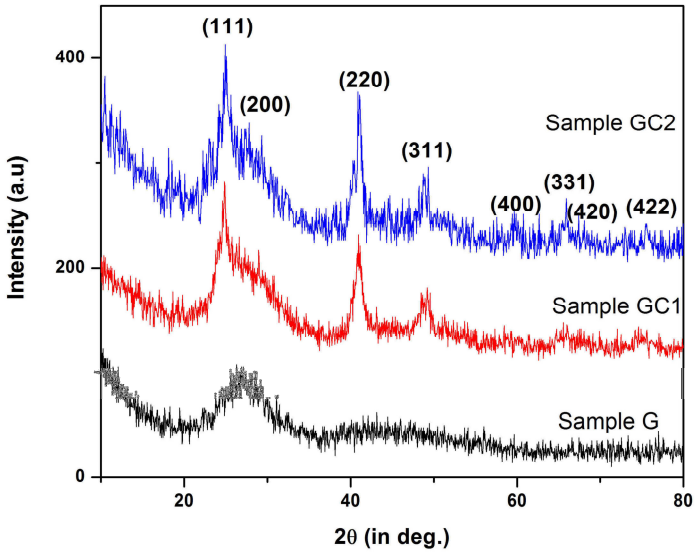
(111)
(200)
(220)
(311)
(400)
(331)
(420)
(422)
Sample GC2
Sample GC1
Sample G
Intensity (a.u)
2θ (in deg.)
0
200
400
20
40
60
80

Fig. 3

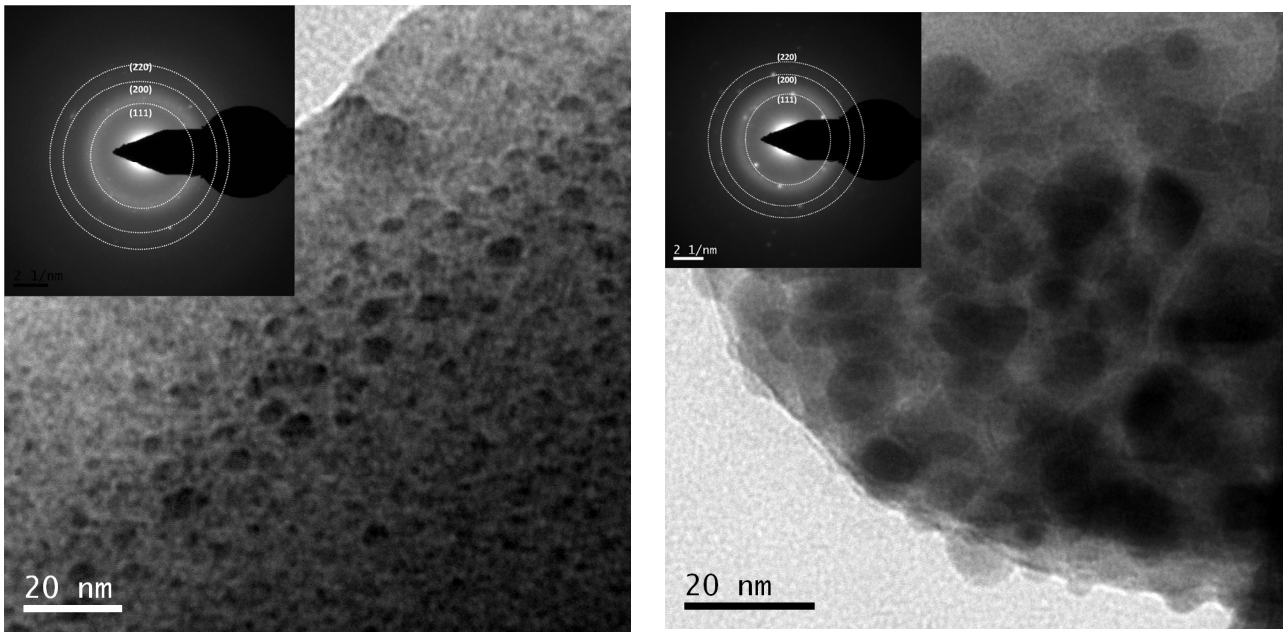

(a) **(b)**

Fig 4

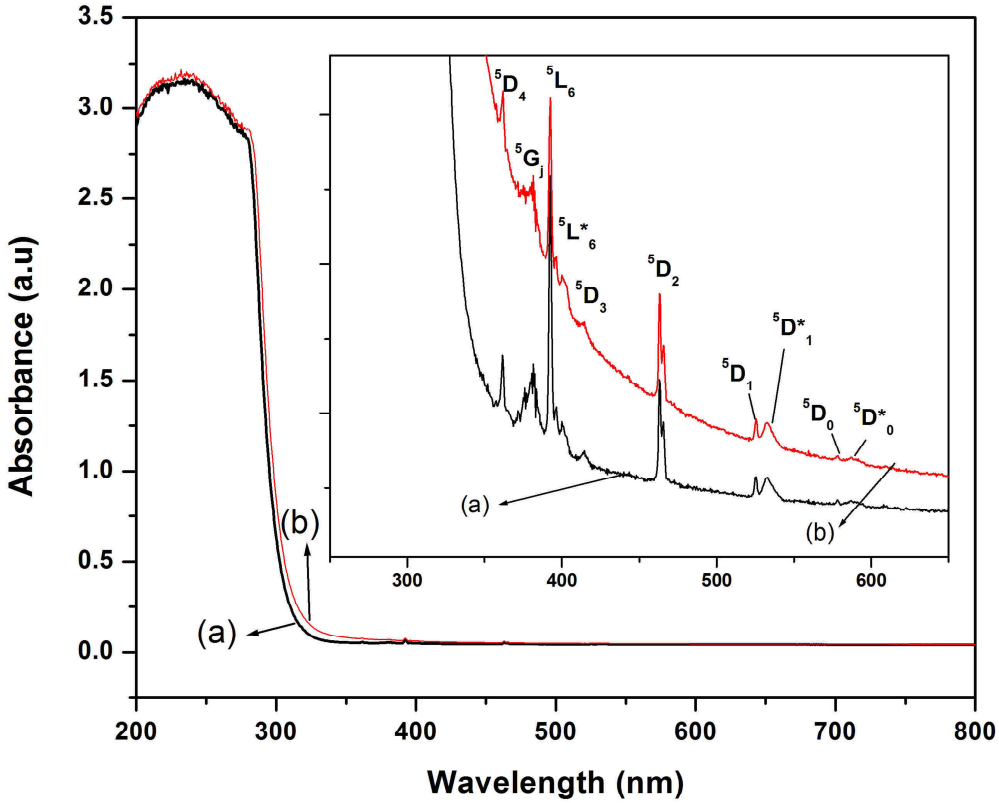
Absorbance (a.u)
Wavelength (nm)
(a)
(b)
$^5D_4$
$^5L_6$
^5G_j
$^5L^*_6$
$^5D_3$
$^5D_2$
$^5D^*_1$
$^5D_1$
$^5D_0$
$^5D^*_0$

Fig 5

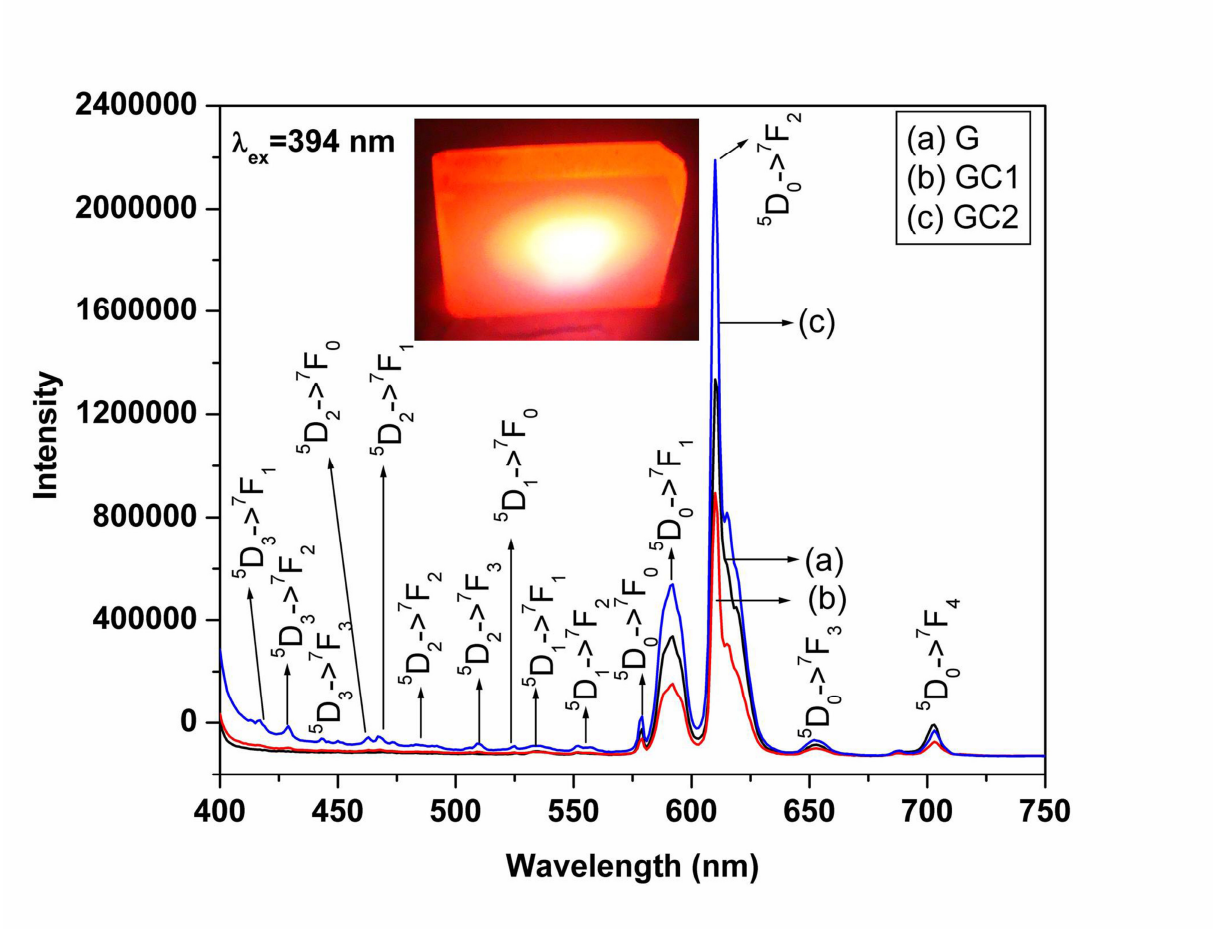
λex=394 nm
(a) G
(b) GC1
(c) GC2
Intensity
Wavelength (nm)
2400000
2000000
1600000
1200000
800000
400000
0
400
450
500
550
600
650
700
750
5D3->7F1
5D3->7F2
5D3->7F3
5D2->7F0
5D2->7F1
5D2->7F2
5D2->7F3
5D1->7F0
5D1->7F1
5D1->7F2
5D0->7F0
5D0->7F1
5D0->7F2
5D0->7F3
5D0->7F4
(a)
(b)
(c)

Fig. 6

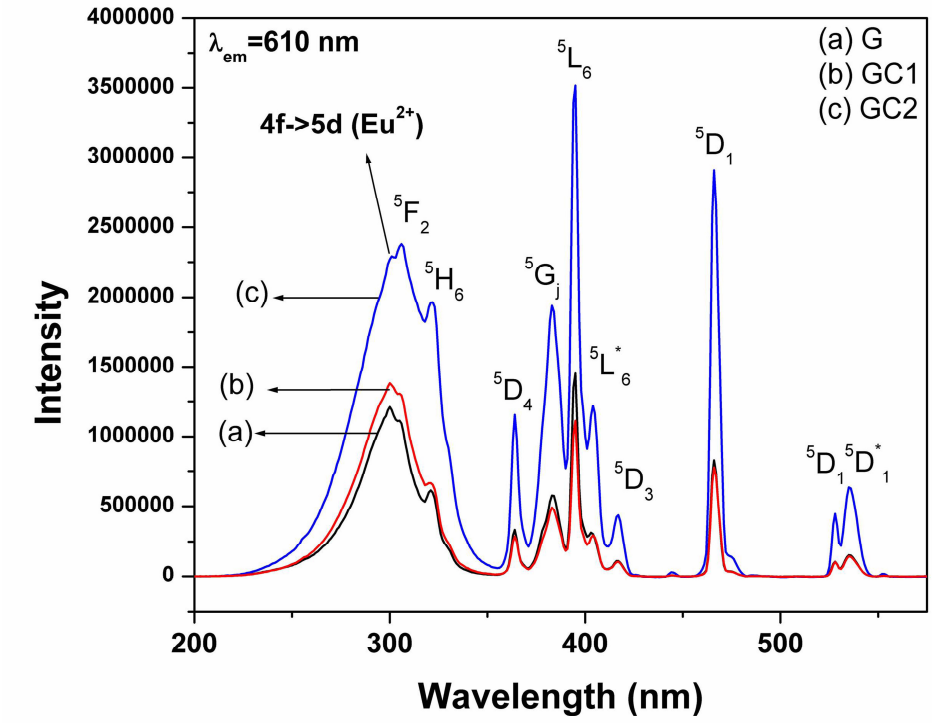
λem=610 nm
4f->5d (Eu2+)
(a) G
(b) GC1
(c) GC2
5F2
5H6
5Gj
5L6
5L*6
5D4
5D3
5D1
5D1 5D*1
(c)
(b)
(a)
Intensity
Wavelength (nm)
4000000
3500000
3000000
2500000
2000000
1500000
1000000
500000
0
200
300
400
500

Fig. 7

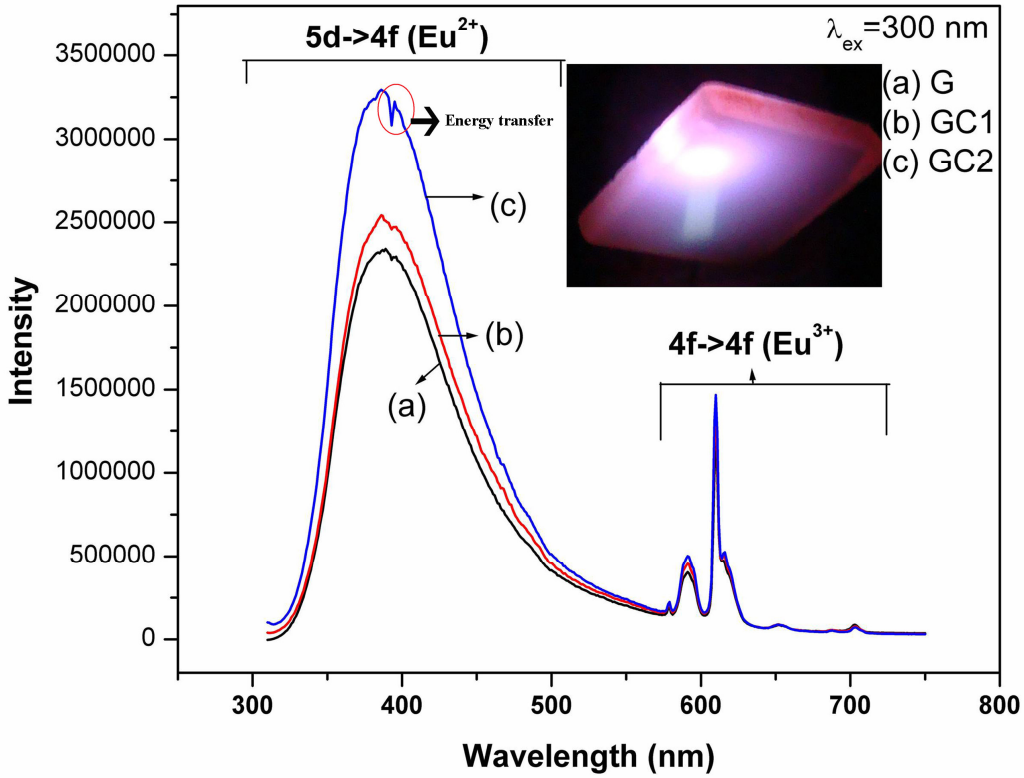
5d->4f (Eu2+)
λex=300 nm
(a) G
(b) GC1
(c) GC2
Energy transfer
(c)
(b)
(a)
4f->4f (Eu3+)
Intensity
Wavelength (nm)
3500000
3000000
2500000
2000000
1500000
1000000
500000
0
300
400
500
600
700
800

Fig. 8

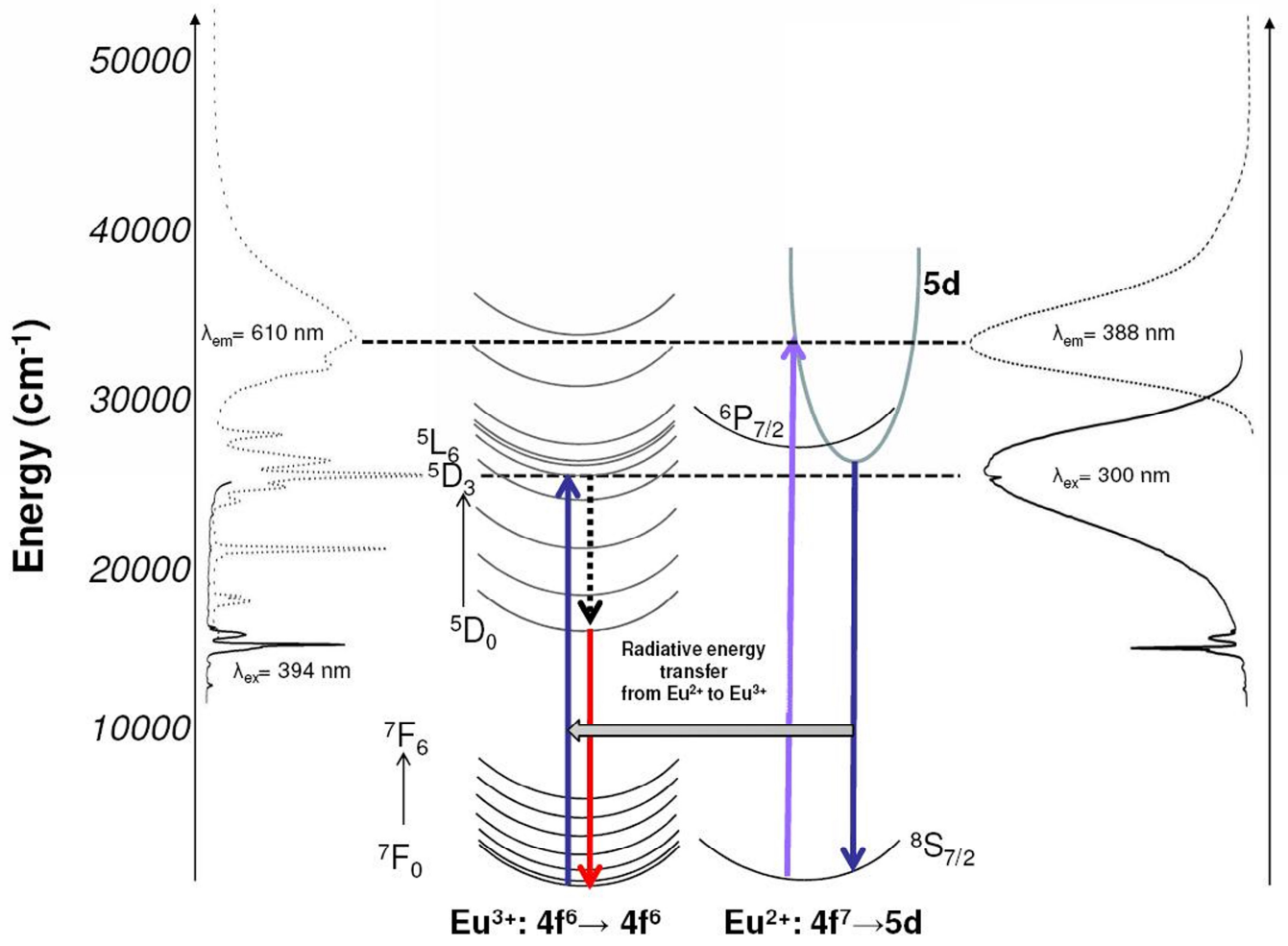
Energy (cm-1)
50000
40000
30000
20000
10000
λem= 610 nm
λem= 388 nm
λex= 394 nm
λex= 300 nm
5d
6P7/2
5L6
5D3
5D0
Radiative energy
transfer
from Eu2+ to Eu3+
7F6
7F0
8S7/2
Eu3+: 4f6→ 4f6
Eu2+: 4f7→5d

Fig.9